JOURNAL OF MATERIALS SCIENCE 28 (1993) 6799–6808

Dilatational bands in rubber-toughened polymers

A. LAZZERI
Materials Engineering Centre, University of Pisa, Via Diotisalvi 2, 56100 Pisa, Italy
C. B. BUCKNALL
SIMS, Cranfield Institute of Technology, Cranfield, Bedford MK43 OAL, UK

A theory is advanced to explain the effects of rubber particle cavitation upon the deformation and fracture of rubber-modified plastics. The criteria for cavitation in triaxially-stressed particles are first analysed using an energy-balance approach. It is shown that the volume strain in a rubber particle, its diameter and the shear modulus of the rubber are all important in determining whether void formation occurs. The effects of rubber particle cavitation on shear yielding are then discussed in the light of earlier theories of dilatational band formation in metals. A model proposed by Berg, and later developed by Gurson, is adapted to include the effects of mean stress on yielding and applied to toughened plastics. The model predicts the formation of cavitated shear bands (dilatational bands) at angles to the tensile axis that are determined by the current *effective* void content of the material. Band angles are calculated on the assumption that all of the rubber particles in a band undergo cavitation and the effective void content is equal to the particle volume fraction. The results are in satisfactory agreement with observations recorded in the literature on toughened plastics. The theory accounts for observed changes in the kinetics of tensile deformation in toughened nylon following cavitation and explains the effects of particle size and rubber modulus on the brittle–tough transition temperature.

1. Introduction

It has long been recognised that microscopic cavitation processes make an important contribution to the fracture resistance of rubber-toughened polymers, including both plastics and thermosets. Cavitation of toughened plastics was first reported in high-impact polystyrene (HIPS), which absorbs energy principally through multiple crazing of the polystyrene (PS) matrix [1]. It is clear from several transmission electron microscopy (TEM) studies that fibrillation of the PS to form crazes is accompanied by somewhat coarser fibrillation of the rubber phase in the neighbouring particles [2–4], a process that enables the rubber particles to match the high strains in the surrounding matrix. Recently, Kramer *et al.* [5] used real-time X-ray measurements on HIPS to show that cavitation of the rubber particles actually precedes crazing of the matrix under tensile impact conditions. Cavities formed within the rubber particles can thus be seen as nuclei for craze growth, which occurs through the meniscus-instability mechanism proposed by Argon and Salama [6].

Rubber particle cavitation is also of critical importance for toughening of plastics that are resistant to crazing. This was first recognised by Breuer *et al.* [7], who combined TEM with low-angle light scattering to study deformation mechanisms in ABS and rubber-modified PVC. They observed X-shaped light-scattering patterns, which are consistent with the formation of planar cavitated shear bands having their normals at about 35° to the tensile axis. Fibrillation of a continuous rubber phase in toughened PVC has been reported by Michler [8].

Cavitation of the rubber particles has also been seen in a number of other toughened polymers, notably epoxy resins containing CTBN rubber [9–11] and nylon–rubber blends [12]. Recently, Yee and Pearson have employed optical microscopy to observe particle cavitation in toughened epoxy resins [13] and shown that this precedes large-scale shear yielding of the matrix. Furthermore, Borggreve and Gaymans have shown that the brittle–tough transition in rubber-toughened nylon 6 shifts to higher temperatures when rubbers of increasing shear modulus (and hence increasing cavitation resistance) are used as toughening agents [14]: this work supports the view that particle cavitation is a prerequisite for extensive shear yielding of the matrix polymer under the severe conditions of the notched impact test. The same authors have shown that the brittle–tough transition temperature in toughened nylon decreases with decreasing particle size, but only down to a limiting diameter of about 0.2 μm, below which the rubber particles appear to be very difficult to cavitate [15].

Direct TEM evidence of cavitation in toughened nylons has been published by Ramsteiner *et al.* [16, 17], and comparable SEM observations have been made by Speroni *et al.* [18], Bucknall *et al.* [19] and Dijkstra [20]. Both Ramsteiner and Speroni showed that the voids were associated preferentially with shear bands.

0022–2461

These studies demonstrate that expansion, interaction and eventual coalescence of voids, following cavitation of the rubber particles, play a central role in the fracture behaviour of many rubber-toughened polymers, including epoxy resins, polyamides and other craze-resistant polymers. This role is clearly important in allowing the toughened polymer to reach high plastic strains within the zone of high triaxial stress around a crack tip. The present paper examines the criteria for rubber particle cavitation and the effects of cavitation on the subsequent yield behaviour of a non-crazing toughened polymer.

2. A model for rubber particle cavitation

There is no established criterion for cavitation in rubber particles. The fracture mechanics model of Gent [21] is not really appropriate because it deals with bulk samples of rubber, which contain defects (contaminant particles, etc) with sizes in the range 0.5 μm to ~ 1 mm. The rubber particles in toughened grades of epoxy resin and nylon have diameters of the order of 0.5 μm and it is very unlikely that every particle contains a defect of this size.

An alternative model is outlined below. Its basic assumptions are: (a) that the largest defects within a typical rubber particle under triaxial tension are microvoids with dimensions of the order of a few nanometres; and (b) that these microvoids will expand only if the resulting release of stored volumetric strain energy is sufficient both to increase the surface area of the void and to stretch the surrounding layers of rubber.

For convenience of calculation the void is assumed to be a sphere of radius r lying at the centre of a spherical rubber particle of radius R, which is well bonded to the matrix. If cavitation is initiated at a critical mean stress σ_{mc}, the strain energy of the particle immediately before initiation is given by

$$U_0 = \frac{4}{3}\pi R^3 W^* = \frac{2}{3}\pi R^3 K \Delta_{V0}^2 \quad (1)$$

where W^* is the stored energy density of the rubber, K is its bulk modulus and Δ_{V0} is the volume strain within the rubber phase immediately before cavitation. The radius of the particle is assumed to remain constant during the expansion of the cavity, so that no additional external work is done on the particle by the matrix. In relation to the rubber particle, the volume fraction of the cavity is r^3/R^3 and the resulting volume strain within the cavitated rubber phase is therefore $(\Delta_{V0} - r^3/R^3)$.

The formation of a cavity introduces two additional contributions to the energy of the rubber particle: a surface energy $4\pi r^2\Gamma$, where Γ is the surface tension of the rubber; and the shear strain energy, $\int W_s^* dV$, required to stretch the rubber and allow the cavity to expand. The total energy U of the cavitated particle is then given by

$$U = \frac{2}{3}\pi R^3 K\left(\Delta_{V0} - \frac{r^3}{R^3}\right)^2 + 4\pi r^2\Gamma + \int W_s^* dV \quad (2)$$

A typical value of Γ for a hydrocarbon elastomer is 0.03 N m^{-1} [22].

In order to calculate the shear strain energy density term W_s^* we use the standard equation of rubber-like elasticity theory:

$$W_s^* = \frac{G}{2}(\lambda_1^2 + \lambda_2^2 + \lambda_3^2 - 3) \quad (3)$$

The formation of the cavity causes a concentric rubber shell of radius a to undergo equibiaxial stretching to a final radius b. The principal extension ratios are then $\lambda_1 = \lambda_2 = \lambda$ and $\lambda_3 = \lambda^{-2}$, where $\lambda = b/a$. This gives

$$W_s^* = \frac{G}{2}(2\lambda^2 + \lambda^{-4} - 3) \quad (4)$$

If ρ_a, ρ_b are the densities of the rubber phase before and after cavitation, then the relationship between the extension λ of a thin spherical shell and its radial distance b from the centre of the cavitated particle is

$$\rho_a a^3 = \rho_b(b^3 - r^3) \quad (5)$$

which on rearranging gives

$$b = a\lambda = r\lambda\left(\lambda^3 - \frac{\rho_a}{\rho_b}\right)^{-1/3} \quad (6)$$

Noting that $dV = 4\pi b^2\, db$, the following expression can now be obtained for the shear strain energy U_s of the cavitated particle

$$U_s = \int_{b=r}^{R} 4\pi b^2 W(b) db \quad (7)$$

Combining Equations 4, 6 and 7 then gives

$$U_s = 2\pi r^3 \rho G \int_{\lambda=\lambda_f}^{1} \frac{\lambda^2(2\lambda^2 + \lambda^{-4} - 3)}{(\lambda^3 - \rho)^2} d\lambda \quad (8)$$

where ρ represents the density ratio ρ_a/ρ_b, which generally lies between 0.99 and 1.0, and λ_f is the extension ratio of the rubber at failure in equibiaxial tension. Equation 8 can be written in abbreviated form

$$U_s = 2\pi r^3 \rho G F(\lambda_f) \quad (9)$$

Numerical integration shows that $F(\lambda_f)$ increases from 0.7 to 1.3 over the range of λ_f values from 2 to 6. Reported values of λ_f for vulcanised natural rubber in equibiaxial tension are between 3.5 and 4.0 [23].

The above treatment neglects the small volume of rubber at the centre of the particle which is stretched beyond λ_f and fails. Writing a_f for the radius of this zone and W_{sf}^* for the shear strain energy density at failure, and using the expression for a from Equation 6, the energy required to rupture this region is given by

$$U_{sf} = \frac{4}{3}\pi a_f^3 W_{sf}^* = \frac{4\pi r^3 W_{sf}^*}{3(\lambda_f^3 - \rho)} \quad (10)$$

As both U_s and U_{sf} are proportional to r^3 they can be combined into a single expression, with a suitable modification of $F(\lambda_f)$. The final expression for the

energy of a cavitated particle is then

$$U = \frac{2}{3}\pi K R^3\left(\Delta_{VO} - \frac{r^3}{R^3}\right)^2 + 4\pi r^2\Gamma + 2\pi r^3 G\rho F(\lambda_f) \quad (11)$$

or

$$U = \frac{2}{3}\pi K R^3\left[\left(\Delta_{VO} - \frac{r^3}{R^3}\right)^2 + \frac{6\Gamma}{KR}\frac{r^2}{R^2} + \frac{3G\rho F(\lambda_f)}{K}\frac{r^3}{R^3}\right] \quad (12)$$

If the initial volume strain in the rubber phase Δ_{VO} is sufficiently high, this function passes through a very minor maximum at small r, followed by a more pronounced minimum as the volume strain due to the cavity r^3/R^3 approaches the original dilatational strain in the rubber phase. From Equation 12 it can be seen that the importance of the surface energy term in relation to the total energy U decreases as the particle radius R increases, with the result that lower values of Δ_{VO}, and therefore of applied stress, are required to cavitate the particle. Fig. 1 illustrates the effect of keeping the volume strain Δ_{VO} constant and varying R. The data are plotted in terms of the reduced variables U/U_0 and r/R, where U_0 is the energy of the strained particle immediately before cavitation (Equation 1). The calculations are based on a rubber with shear modulus $G = 0.4$ MPa, bulk modulus $K = 2000$ MPa, surface tension $\Gamma = 0.03\ \mathrm{N\,m^{-1}}$, $\rho = 1.0$ and $F(\lambda_f) = 1.0$, with the initial volume strain in the particle set at 0.4%. It is clear that only particles with $R > 125$ nm will cavitate under these conditions.

3. Yielding with plastic dilatation

As noted in the Introduction, there is evidence from a number of laboratories that rubber particle cavitation in several different polymers is concentrated within regions of high shear strain. Similar cavitated yield zones have been reported in the metals literature, where they are termed 'dilatation bands'. A recent book by Thomason critically reviews the models that have been proposed to describe the formation and failure of dilatational bands in steels and other ductile metals [24].

Although there are many similarities between ductile metals and polymers, there are also important differences. In particular, polymers exhibit a much greater ability to extend and strain harden, through the process of molecular orientation. Whereas cavitation in metals often causes a reduction in ductility because the voids coalesce at moderate strains, cavitation in polymers is stabilised by orientation hardening and strengthening, allowing energy absorbing internal necking to take place extensively throughout the stressed region.

The effects of nucleation and growth of microvoids on the yield behaviour of ductile polymers are analysed below using the constitutive equations for a porous ductile material developed by Gurson [25] on the basis of previous work by Berg [26]. These authors adopted a continuum approach to materials undergoing plastic deformation accompanied by void formation. Their model, which is directed essentially at describing the yield behaviour of ductile metals, is reviewed briefly below and the modifications necessary in applying it to polymers are then discussed.

In order to understand the kinetics of yielding it is necessary to relate the macroscopic response of the polymer to its microscopic behaviour. At the macroscopic level we consider an element of ductile polymer containing a large number of microvoids, sufficient to enable it to be treated as homogeneous, as illustrated in Fig. 2. The term 'macroscopic' refers to average values of physical properties (stress, strain, etc.) of the voided element and 'microscopic' refers to the properties of the matrix at individual points around the voids.

For a homogeneous rigid–plastic material, in which pressure has no effect upon yielding, the von Mises yield criterion can be written (indices range from 1 to 3, δ_{ij} represents the Kroneker delta and repeated indices indicate summation)

$$\frac{3}{2}s_{ij}s_{ij} = \sigma_y^2 \quad (13)$$

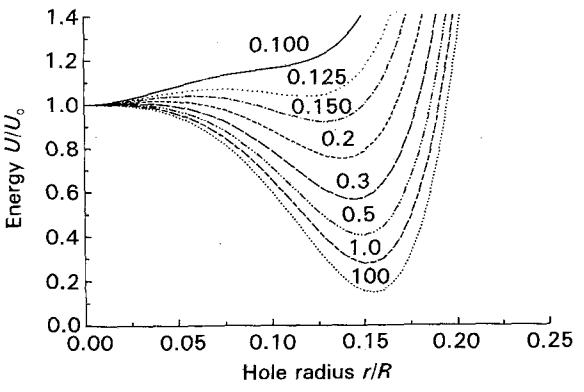

Figure 1 Calculated potential energy of a cavitated rubber particle as a function of the reduced radius of the void, r/R, for particles of radius R in the range 0.1–100 μm. Values calculated using Equation 12 with fixed volume strain $\Delta_{VO} = 0.004$.

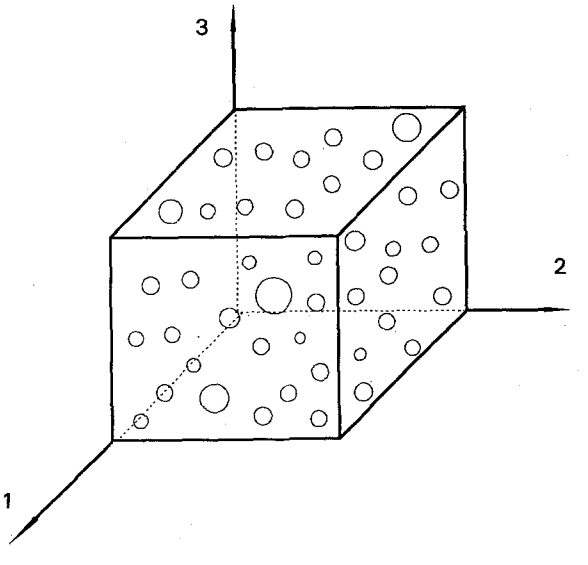

Figure 2 Element of ductile material containing a large number of microvoids.

where σ_y is the tensile yield stress, the stress deviator s_{ij} is related to the stress components σ_{ij} by the relation

$$s_{ij} = \sigma_{ij} - \frac{1}{3}\sigma_{kk}\delta_{ij} \quad (14)$$

and the mean stress σ_m (sometimes called hydrostatic stress or negative pressure) is given by

$$\sigma_m = \frac{\sigma_{kk}}{3} = \frac{\sigma_1 + \sigma_2 + \sigma_3}{3} = -p \quad (15)$$

where p is pressure. The von Mises equivalent stress is defined as

$$\sigma_e = \sqrt{(\sigma_1 - \sigma_2)^2 + (\sigma_2 - \sigma_3)^2 + (\sigma_3 - \sigma_1)^2/2)}$$

$$\sigma_e = \sqrt{\frac{3}{2}s_{ij}s_{ij}} \quad (16)$$

If the cartesian axes coincide with the three principal directions Equation 13 can be written.

A yield function describes the locus in stress space of points for which the material will undergo plastic yield. The following simple yield function Φ can be derived from Equations 13 and 16 for a von Mises material

$$\Phi = \frac{\sigma_e^2}{\sigma_y^2} - 1 = 0 \quad (17)$$

Several studies have demonstrated clearly that pressure affects the yield behaviour of polymers [27–29]. This is most easily seen in comparisons between σ_C and σ_T, the compressive and tensile values of uniaxial yield stress: for many ductile plastics $\sigma_C/\sigma_T \approx 1.3$. The experimental data can be correlated by introducing an additional pressure-dependent term into the von Mises criterion [28, 29]

$$\sigma_e^2 = (\sigma_0 - \mu\sigma_m)^2 \quad (18)$$

where σ_0 is the yield stress in the absence of any overall hydrostatic pressure and μ is a dimensionless material constant, which characterizes the pressure sensitivity of yielding. It is related to σ_C and σ_T by:

$$\mu = 3\left(\frac{\sigma_C - \sigma_T}{\sigma_C + \sigma_T}\right) \quad (19)$$

where $\mu \approx 0.39$ for many polymers. The yield function (Equation 17) must also be modified to take account of the pressure dependence. Expansion of Equation 18 gives

$$\Phi(\sigma_e, \sigma_m) = \frac{\sigma_e^2}{\sigma_0^2} + g(\sigma_m) - 1 = 0 \quad (20)$$

where

$$g(\sigma_m) = \frac{\mu\sigma_m}{\sigma_0}\left(2 - \frac{\mu\sigma_m}{\sigma_0}\right) \quad (21)$$

describes the pressure dependence of the yield function. Fig. 3 shows the effects of the mean stress on the yield locus. The yield surface is a cone in stress space, which intersects the 1-2, 1-3 and 2-3 planes to form distorted ellipses. For $\mu = 0$, $g(\sigma_m) = 0$, and the yield function coincides with that for a pressure-independent von Mises material, for which the yield surface is a circular cylinder.

For a pressure-independent material containing spherical voids, Gurson [25] found the following expression for the yield function:

$$\Phi = \frac{\sigma_e^2}{\sigma_y^2} + 2f\cosh\left(\frac{3\sigma_m}{2\sigma_y}\right) - f^2 - 1 = 0 \quad (22)$$

where f is the current volume fraction of voids. The equivalent and mean stresses, σ_e and σ_m, are now 'macroscopic' quantities, whilst σ_y is the (microscopic) matrix flow stress. Equations 20–22 can be combined to give the following yield function for a pressure-dependent material containing spherical voids

$$\Phi = \frac{\sigma_e^2}{\sigma_0^2} + \frac{\mu\sigma_m}{\sigma_0}\left(2 - \frac{\mu\sigma_m}{\sigma_0}\right) + 2f\cosh\left(\frac{3\sigma_m}{2\sigma_0}\right) - f^2 - 1 = 0 \quad (23)$$

where σ_0, as defined by Equation 18, replaces the tensile yield stress σ_y. Only for pressure-independent materials is $\sigma_0 = \sigma_y$.

Gurson's analysis can thus be adapted to model a cavitating polymer. Fig. 4 shows sections through

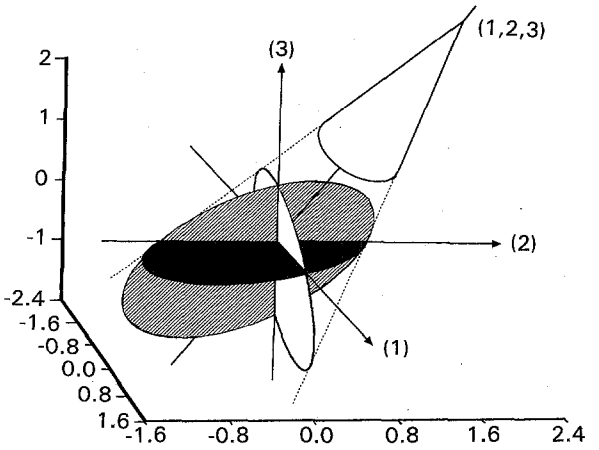

Figure 3 Pressure-modified von Mises yield surface in adimensional principal stress space for a non-cavitating polymer with $\mu = 0.39$. (1), (2) and (3) are the principal stress axes, and (1, 2, 3) is the space diagonal.

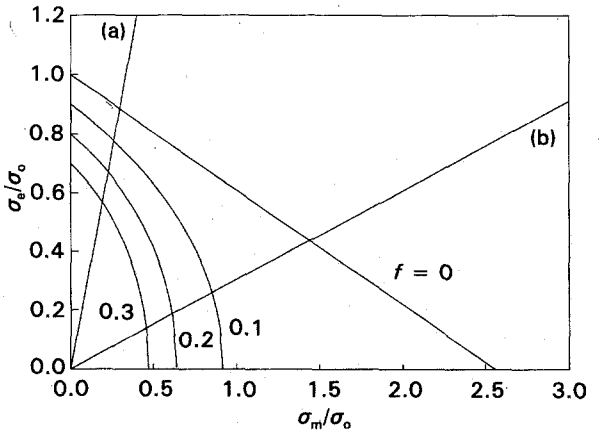

Figure 4 Effect on the yield locus of a pressure dependent material ($\mu = 0.39$) as the void volume fraction f is varied between 0 and 0.3. (a) Uniaxial tension; (b) crack tip plane strain tension.

four yield surfaces, calculated using Equation 23, for materials with $f = 0$, 0.1, 0.2 and 0.3. In this diagram the abscissa lies along the stress-space diagonal defined by $\sigma_1 = \sigma_2 = \sigma_3$ and the distance of any point on the diagram from the space diagonal indicates the magnitude of the effective stress σ_e. The calculations show that an increase in void volume fraction causes additional curvature of the yield surface, so that the apex of the original cone, which represents yielding of a fully-dense polymer, becomes rounded when voids are present. It is clear that, in the presence of microvoids, the yield condition is reached well before the macroscopic equivalent stress equals the matrix flow stress, even when the mean stress σ_m is low or zero. Furthermore, under the plane strain conditions prevailing ahead of a crack tip, where σ_m is initially high compared with σ_e, the absolute values of stress at yield are very much reduced when the polymer is able to cavitate.

Fig. 5 presents the results of calculations based on Equation 23 which illustrate the effects of void volume fraction on: (a) $\sigma_{ty}(f)/\sigma_{ty}(0)$, the adimensional yield stress under uniaxial tension; and (b) $\sigma_{ey}(f)/\sigma_{ey}(0)$, the adimensional effective stress at yield at a point immediately ahead of a sharp crack. The latter calculation is based on a polymer with Poisson's ratio $\nu = 0.4$, with the crack tip in plane strain. The results emphasise the point that cavitation has a more significant effect on yielding at a crack tip than it does in a specimen subjected to uniaxial tension.

The volume fraction of voids may vary during deformation. This can be taken into account by considering the rate of increase of the void volume fraction:

$$\dot{f} = \dot{f}_{\text{growth}} + \dot{f}_{\text{nucleation}} \tag{24}$$

As the volume of the matrix polymer itself does not change with plastic deformation, the rate of change of the total volume is directly proportional to the rate of void growth [30, 31]

$$\dot{f}_{\text{growth}} = (1-f)\dot{\varepsilon}^{p}_{kk} \tag{25}$$

In order to relate the stress components at yielding to the plastic strain increment it is necessary to determine a *flow* rule. In general this can be done by defining a plastic potential, i.e. a function of stress (at yielding) which relates the direction of plastic flow to the shape of the yield surface in stress space. In the conventional theory of plasticity the yield function Φ is used as a plastic potential [32]

$$\dot{\varepsilon}^{p}_{ij} = \Lambda\frac{\partial\Phi}{\partial\sigma_{ij}} \tag{26}$$

where Λ is a macroscopic scalar quantity that can be taken to denote an *effective stretching* and is, in general, a function of stress, stress rate, deformation history and void volume fraction [33].

In the case of polymeric materials the yield function Φ is dependent upon hydrostatic pressure and the condition

$$\frac{\partial\Phi}{\partial\sigma_{ij}} = 0 \tag{27}$$

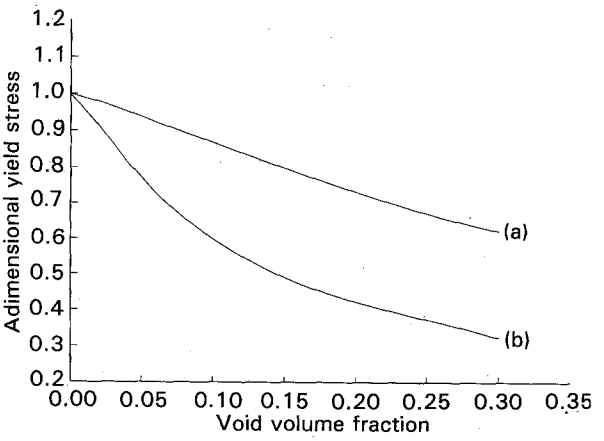

Figure 5 Effect of void volume fraction on: (a) the adimensional tensile yield stress $[\sigma_{ty}(f)/\sigma_{ty}(0)]$ and (b) the adimensional effective stress at yield $[\sigma_{ey}(f)/\sigma_{ey}(0)]$, according to the modified Gurson model.

is not satisfied. Therefore, on the basis of the mathematical theory of plasticity, a volume change is expected to accompany plastic deformation. However, several experimental studies, reviewed by Bowden [34] and Ward [35], have clearly indicated that in the absence of cavitation, flow after yield occurs at essentially constant volume or with a very limited increase in volume. Moreover, as discussed by Bowden and Ward, in polymers it is not necessary to invoke a continuously increasing plastic dilatation or a violation of St Venant's principle (for isotropic materials, the principal axes of stress and plastic strain rate coincide) to explain the pressure dependence of flow stress, because compression significantly reduces molecular mobility and so increases the yield stress. From the above discussion it appears that the normality rule applies to isotropic polymers [33], so that the yield function Φ can be used as a plastic potential.

As Berg [26] and Gurson [25] have stated, following a previous comment by Bishop and Hill [36, 37], the local validity of the normality rule for the ductile matrix material implies that the same normality rule applies macroscopically. From Equation 26 it follows that

$$\begin{aligned}\dot{\varepsilon}^{p}_{ij} &= \Lambda\frac{\partial\Phi}{\partial\sigma_{ij}} \\ &= \Lambda\left[\frac{\partial\Phi}{\partial\sigma_e}\frac{\partial\sigma_e}{\partial\sigma_{ij}} + \frac{\partial\Phi}{\partial p}\frac{\partial p}{\partial\sigma_{ij}} + \frac{\partial\Phi}{\partial\sigma_0}\frac{\partial\sigma_0}{\partial\sigma_{ij}} + \frac{\partial\Phi}{\partial f}\frac{\partial f}{\partial\sigma_{ij}}\right]\end{aligned} \tag{28}$$

If nucleation is neglected, this equation can be simplified. Moreover, for non-hardening materials, $d\sigma_0 = 0$ and Equation 28 can therefore be written (see Appendix I)

$$\dot{\varepsilon}_{ij} = \Lambda\left[\frac{3}{2}\frac{s_{ij}}{\sigma_0} + \alpha\delta_{ij}\right] \tag{29}$$

where

$$\alpha = \frac{\mu}{3}\left[1 - \mu\frac{\sigma_m}{\sigma_0}\right] + \frac{f}{2}\sinh\left[\frac{3\sigma_m}{2\sigma_0}\right] \tag{30}$$

The Berg–Gurson model has been reviewed by Thomason [24], who has proposed a modified approach which takes into account the stress concentrations in ligaments between cavities and the resulting necking of these ligaments. The predictions of the modified model are in better agreement with the observed relationships between void contents and true strains to failure in ductile metals. Thomason's objections to the validity of the Berg–Gurson model do not appear to be applicable to polymer-based materials, since internal necking in the ligaments between cavitated rubber particles is not followed by void coalescence, which occurs only at very high strains in ductile polymers. The modified Berg–Gurson model outlined above appears therefore to be a realistic one for representing the deformation behaviour of a polymer containing microvoids.

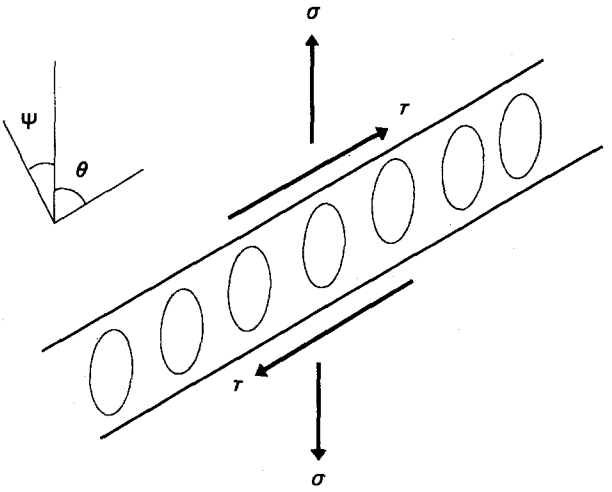

Figure 6 Schematic representation of a dilatational band.

4. Deformation in plane plastic strain—dilatational bands

When an element of material is restrained in two dimensions the only types of deformation compatible with the constraint are simple shear parallel to the plane and volume dilatation normal to it. Where both are present, the result is a dilatation band, as illustrated in Fig. 6. The conditions for development of such a band in a porous plastic polymeric material will be examined following the approach proposed by Berg [26].

Defining the plane of deformation illustrated in Fig. 6 as the 1-2 plane we can write

$$\dot{\varepsilon}_{13} = \dot{\varepsilon}_{23} = \dot{\varepsilon}_{33} = \sigma_{13} = \sigma_{23} = 0 \quad (31)$$

Applying Equation 29 to the 33 (zero strain rate) direction and substituting for s_{33} using Equation 14

$$\sigma_{33} = \frac{(\sigma_{11} + \sigma_{22})}{2} - \alpha\sigma_0 \quad (32)$$

The angle of the dilatational bands can be determined as shown in Fig. 7, using the Mohr's circle construction. The circle shown is for the direct stresses σ_1, σ_2 and shear stress τ. A second Mohr's circle can be constructed for *deviatoric* stress components in the plane of deformation, by subtracting the mean stress from the normal stress components. From Equations 15 and 32 σ_m is given by:

$$\sigma_m = \frac{(\sigma_{11} + \sigma_{22})}{2} - \frac{\alpha\sigma_0}{3} \quad (33)$$

The new Mohr's circle has the same diameter as the original one and is formed simply by moving the origin of the stress plane (Fig. 7) onto the line a–a. This involves a displacement from the centre of the circle of $\alpha\sigma_0/3$. A third Mohr's circle, for strain increments, $2\varepsilon^p_{ij}\sigma_0/3\Lambda$ can now be obtained by shifting the origin of this diagram to the left of a–a by the distance $2\alpha\sigma_0/3$ (Equation 29). In Fig. 7 the origin of the Mohr's circle of plastic strain increments lies on the line b–b. The intersection of the line b–b with the Mohr's circle of Fig. 7 therefore identifies the location of the 2′3 planes, for which extension rates in the

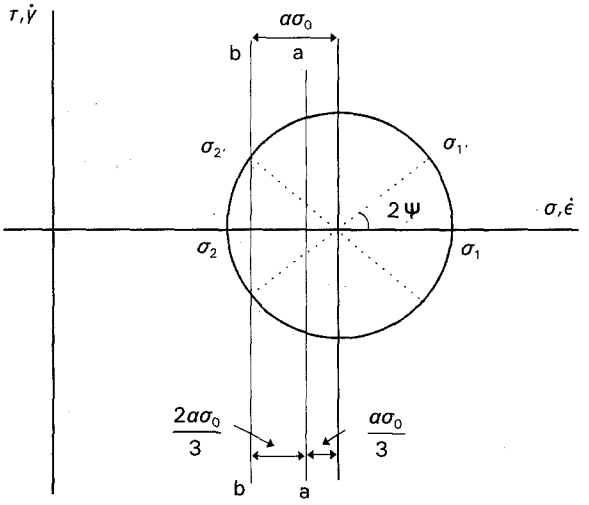

Figure 7 Mohr's circle constructions for stress and plastic strain rate.

normal 2′2′ and 33 directions vanish and extension is limited to the 1′1′ direction, normal to the plane. For these planes

$$\sigma_{1'1'} - \sigma_{2'2'} + 2\alpha\sigma_0 = 0 \quad (34)$$

Hence, from the Mohr's circle construction, the angle of inclination θ of the dilatational band with respect to the major principal stress axis is given by:

$$\cos 2\theta = -\frac{2\alpha\sigma_0}{\sigma_1 - \sigma_2} \quad (35)$$

There is no discussion in the literature concerning the orientations of dilatational bands in polymers, but a number of papers give data on the orientations of (void-free) shear bands in pressure-dependent materials, which provide a basis for comparison with Equation 35. If the material contains no voids and has $\mu = 0$, then $\alpha = 0$ and $\theta = 45°$. Equation 35 predicts that in polymers the inclination of shear band normals to the major principal stress axis deviates from 45°, because $\mu \neq 0$. For solid polymers with $f = 0$, Equation 35 can be written

$$\cos 2\theta = -\frac{2\mu(\sigma_0 - \mu\sigma_m)}{3\cdot\ \sigma_1 - \sigma_2} \quad (36)$$

In uniaxial tension, $\sigma_1 = \sigma_{yt} = \sigma_0/(1 + \mu/3)$ and $\sigma_2 = \sigma_3 = 0$. Taking $\sigma_C/\sigma_T = 1.33$ ($\mu = 0.425$) for rigid PVC, Equation 36 predicts $\theta = 53.2°$ ($\cos 2\theta = -2\mu/3$), which is in good agreement with the experimental value of 55° measured for PVC samples deformed in tension [38] and for thin-walled tubes deformed in tension and torsion [39]. In plane strain compression, where $\sigma_1 = -\sigma_{yc} = -\sigma_0/(1 - \mu/2)$, $\sigma_2 = 0$ and $\sigma_3 = \sigma_m = -\sigma_{yc}/2$, Equation 36 gives $\theta = 36.8°$($\cos 2\theta = 2\mu/3$) and $\Psi = 53.2°$, which may be compared with an experimental value of $\Psi = 49°$ [40].

Better agreement is found for bands formed in plane-strain compression tests on polystyrene ($\mu = 0.39$). Equation 36 gives a value of $\Psi = 52.5°$, whilst Argon *et al.* [41] measured a value of 53° for bands formed in compression near a stress-concentrating notch. An identical value was obtained by Bowden and Jukes [40] in a plane-strain compression test.

The effect of introducing voids into deformation bands is to increase the pressure sensitivity of the yield criterion, as indicated by Equation 23. Consequently, normals to the bands should rotate towards the major principal stress axis. Values of Ψ calculated according to Equation 35 are given in Fig. 8 as a function of f, the volume fraction of voids within the band, for a typical polymer with $\mu = 0.39$. The calculations show that as f is increased from 0 to 0.34, the angle Ψ decreases from about 38° to 25°. These results are consistent with the band angles observed by Yee and Pearson in optical microscopy studies on toughened epoxy resins [13], in Speroni *et al.*'s SEM work on toughened nylons [18] and in Breuer *et al.*'s light scattering observations on toughened PVC [7]. When the microvoid volume fraction is above 0.5, the band angle drops to zero. This is consistent with the experimental observations of Kambour [42, 43] and of Donald and Kramer [44] that the volume fraction of polymer in fully-stressed crazes is less than 0.5.

From a consideration of Mohr's circle of strain rate (Fig. 7), the ratio of the shear strain rate $\dot{\gamma}$ to the normal strain rate $\dot{\varepsilon}$ is related to the angle Ψ by

$$\tan 2\Psi = \frac{\dot{\gamma}}{\dot{\varepsilon}} \qquad (37)$$

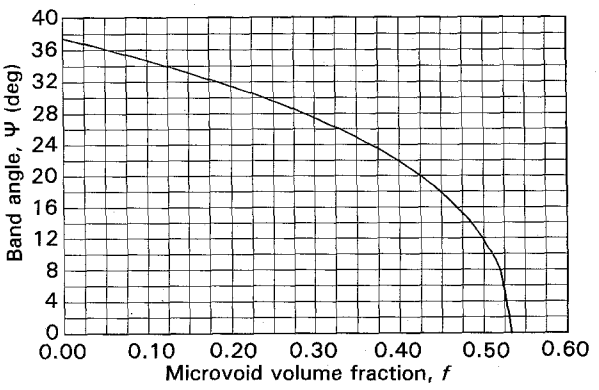

Figure 8 Angle Ψ between the dilatational band normal and the major tensile axis as a function of the volume fraction of microvoids, according to the modified Berg–Gurson model (for a polymer with $\mu = 0.39$).

Thus when $\dot{\gamma} = 0$, then $\Psi = 0$, as in craze formation. On the other hand, when $\dot{\varepsilon} = 0$, then $\Psi = 45°$, which defines an ideal shear band in a von Mises (pressure insensitive) ductile solid.

5. Discussion

As noted in the Introduction, several authors have observed cavitation within the rubber particles of toughened plastics and some, including Ramsteiner *et al.* [16, 17], Speroni *et al.* [18], Sue [11] and Dijkstra [20], have pointed out that the voids observed are associated with shear or deformation bands. The present paper has reviewed evidence presented in these and other publications which shows that the formation of dilatational bands occurs widely in rubber-toughened plastics. There are good reasons for expecting it to occur in most rubber-toughened polymers, especially when the polymer is under constraint and cavitational stresses and strains within the rubber particle are therefore relatively high.

The work of Yee and Pearson on rubber-toughened epoxy resins has shown that particle cavitation begins at an early stage in the deformation [9, 10]. Initially the process appears to occur throughout the crack tip process zone, with no particular correlation between sites. Where there is a distribution of particle sizes, this pattern of cavitation is to be expected from Equation 12, which predicts an inverse relationship between σ_{mc}, the critical mean stress at cavitation, and R, the radius of the rubber particle. In a sample subjected to increasing applied stress, the effective concentration of voids will increase as a result of both initiation and growth of cavities, until the combination of applied stress and void content satisfies Equation 23. Dilatational bands will then form in regions of high void content and propagate along planes defined by Equation 35.

In the thin sections examined by Yee and Pearson it is difficult to identify dilatational bands under plain light, which simply shows the locations of the voids. Only when polarized light is used to examine the same specimen does the association between voids and deformation bands become evident. This is probably the reason why the formation of dilatation bands has not been recognised widely as a general phenomenon in toughened plastics. The recent work of Sue on cavitation of rubber particles in a lightly cross-linked epoxy resin shows much more clearly that the voids form in well defined planar bands, which Sue calls 'croids' [11]. The other effective technique for identifying dilatation bands is low angle light scattering, which merits further attention as a method for studying deformation behaviour in toughened plastics.

Before cavitation, the stresses on the surface of a rubber particle are determined by its bulk modulus and its volume strain. Cavitation of rubber particles is usually observed when the elastic tensile strain ε_1 in the toughened plastic is between 1% and 3%. Taking Poisson's ratio for plastics as about 0.4, this means that the overall volume strain $\Delta V/V$ in the material is between 0.2% and 0.55%. Because of the higher bulk compliance of rubbers, the volume strain within the rubber phase is probably in the range 0.4–1.0%. For

a rubber with a typical bulk modulus $K = 2.0$ GPa, this corresponds to a mean stress on the rubber at cavitation of between 8 and 20 MPa. Immediately a void has formed, the volume strain within the rubber phase, and therefore also the normal stresses at the surface of the particle, fall approximately to zero, so that the particle effectively becomes a void.

This means, for example, that in a typical toughened nylon containing 20 wt % of functionalised ethylene–propylene copolymer (equivalent to a rubber volume fraction of 26%), the effective void content f in a cavitating shear band could under appropriate conditions reach a value as high as 0.26 before significant drawing occurred in the nylon matrix. From Fig. 8 the corresponding band angle is 29°, in good agreement with the observations of Speroni. At low rates of loading, where cavitation proceeds slowly and begins in the larger particles, the concentration of voids is likely to be substantially smaller and the band angle higher—approaching 38°. On the other hand, relatively small amounts of localised yielding in a region where rubber particles have cavitated can result in a significant increase in effective void content f. This might explain Sue's observation of cavitated shear bands lying approximately normal to the tensile axis in toughened epoxy resins [11]. As the cavitated 'croid' bands are initiated at crack tips, where σ_m is high and σ_e is relatively low, void growth should be relatively rapid, in accordance with Equation 25.

An important difference between rubber particle cavitation in toughened plastics and cavitation of metals, which are the subject of Gurson's analysis, is that rubber particles themselves reduce the yield stress of the polymer, so that replacing them with cavitated particles has a less obvious effect on deformation behaviour in uniaxial tension. The dependence of $\sigma_{ty}(f)/\sigma_{ty}(0)$ on void content, as shown in Fig. 5, is very similar to its expected dependence on rubber volume fraction ϕ, which can be expressed by making σ_0 a function of ϕ. Cavitation of the rubber particles is of greater importance at notch tips, where dilatational yielding is necessary to achieve high strains.

An important feature of the dilatation band model is that it retains a distinction between yielding under plane stress and yielding under plane strain conditions at a crack tip. This is implicit in the use of the von Mises equation as the basis for the model: the addition of extra terms to give Equation 23 does not alter the fact that σ_e, the driving force for yielding, is very different between plane stress and plane strain regions of a given crack. This is an important point, because some authors have concluded that rubber particle cavitation (or alternatively matrix cavitation) sets up a state of plane stress at the crack tip and that this in itself is sufficient to explain rubber toughening. Against this argument must be set the evidence that thickness effects are observed in fracture mechanics tests on a number of toughened plastics. For example, K_C increases linearly with B^{-1}, the reciprocal of specimen thickness, in both toughened polypropylene and HIPS [45, 46]. Equation 23 offers a more coherent explanation of toughening, which accounts for these thickness effects.

The matrix ligaments between cavitated particles are subjected to both shear and mean stresses which vary rapidly from point to point. At the matrix–rubber boundary the normal stresses are close to zero, as noted earlier, whereas at the centre of the ligament the stresses are more triaxial and mean stresses σ_m are therefore higher. These variations in stress state over very small distances within a polymer ligament are similar to those discussed by Kramer in his analysis of craze fibrils [47]. The gradient of mean stress across an individual ligament $\nabla\sigma_m$ is determined by the normal stress acting on the dilatation band (which determines the mean stress) and by the interparticle spacing D_{ip}

$$\nabla\sigma_m = \frac{2(\sigma_b - \sigma_s)}{D_{ip}} \tag{38}$$

where σ_b and σ_s are the mean stresses at the centre of the matrix ligament and at the interface with the rubber particle, respectively. This gradient in mean stress contributes to the flow rate within the ligaments and might explain the observations of Wu [48, 49] and of Borggreve *et al.* [50, 51] on the importance of interparticle spacing in controlling the brittle–tough transition in toughened nylon.

The dilatational band model can thus explain why cavitation of the rubber particle, accompanied by a very small immediate increase in volume, has a dramatic effect on the kinetics of creep in toughened nylon containing 26 vol % of rubber, as observed by Bucknall *et al.* [19]. Even if every rubber particle in the material cavitated by converting an elastic volume strain of 1% into a void of equivalent volume, the resulting change in overall dimensions of the specimen would be negligible. However, according to the model proposed in this paper the sudden conversion of rubber particles into the mechanical equivalent of voids has the indirect effect of accelerating volume expansion through the formation of dilatational bands.

Finally, it should be noted that cavitated rubber particles behave like voids only during the early stages of the yielding process. As the local strain in the matrix increases, the rubber phase is forced to stretch until it reaches biaxial extension ratios of 3 or more. At this stage the stresses in the rubber become high enough to cause additional strain hardening of the cavitated material, thus preventing premature failure. This aspect of the problem will be explored further in a later paper.

6. Conclusions

This paper has considered the mechanism of cavitation within the rubber phase of toughened plastics and the effects of cavitation on yielding, with particular reference to the formation of dilatational bands. Angles of cavitated shear bands to the tensile axis in polymers predicted by a modified Berg–Gurson model have been compared with observations recorded in the literature. The proposed models for particle cavitation and consequent deformation through the development of dilatational bands account for the effects of

particle size and rubber modulus on the brittle–tough transition in toughened nylons and for changes in the kinetics of deformation following cavitation. The model also throws light on the relationship between toughness and interparticle spacing.

Acknowledgement

The authors thank Prof. Enrico Manfredi for his helpful comments on the manuscript.

Appendix A

Rewriting Equation 23

$$\Phi = \frac{\sigma_e^2}{\sigma_0^2} + \frac{\mu\sigma_m}{\sigma_0}\left(2 - \frac{\mu\sigma_m}{\sigma_0}\right) + 2f\cosh\left(\frac{3\sigma_m}{2\sigma_0}\right) - f^2 - 1 = 0 \quad \text{(A1)}$$

Using the substitutions $T_e = \sigma_e/\sigma_0$ and $T_H = \sigma_m/\sigma_0$ we obtain

$$\Phi = \Phi(T_e, T_H, f) = T_e^2 + \mu T_H(2 - \mu T_H) + 2f\cosh\left(\frac{3}{2}T_H\right) - f^2 - 1 = 0 \quad \text{(A2)}$$

Equation 28 can be written

$$\dot{\varepsilon}_{ij} = \Lambda\frac{\partial\Phi}{\partial\sigma_{ij}} = \Lambda\left[\frac{\partial\Phi}{\partial T_e}\frac{\partial T_e}{\partial\sigma_{ij}} + \frac{\partial\Phi}{\partial T_H}\frac{\partial T_H}{\partial\sigma_{ij}} + \frac{\partial\Phi}{\partial f}\frac{\partial f}{\partial\sigma_{ij}}\right] \quad \text{(A3)}$$

where

$$\frac{\partial\Phi}{\partial T_e} = 2T_e; \quad \frac{\partial T_e}{\partial\sigma_{ij}} = \frac{1}{\sigma_0}\frac{\partial\sigma_e}{\partial\sigma_{ij}} = \frac{3}{2\sigma_0}\frac{s_{ij}}{\sigma_e}$$

$$\frac{\partial\Phi}{\partial T_H} = 2\mu(1 - \mu T_H) + 3f\sinh\left(\frac{3}{2}T_H\right); \quad \frac{\partial T_H}{\partial\sigma_{ij}} = \frac{\delta_{ij}}{3\sigma_0}$$

$$\frac{\partial\Phi}{\partial f} = 2\left[\cosh\left(\frac{3}{2}T_H\right) - f\right]; \quad \frac{\partial f}{\partial\sigma_{ij}} = 0$$

Substituting these partial derivatives into Equation A3

$$\dot{\varepsilon}_{ij} = \Lambda\left[3\frac{s_{ij}}{\sigma_0^2} + \left(2\mu(1 - \mu T_H) + 3f\sinh\left(\frac{3}{2}T_H\right)\right)\frac{\delta_{ij}}{3\sigma_0}\right] \quad \text{(A4)}$$

On incorporating the factor $2/\sigma_0$ into Λ we obtain

$$\dot{\varepsilon}_{ij} = \Lambda\left[\frac{3s_{ij}}{2\sigma_0} + \left(\frac{\mu}{3}\left(1 - \mu\frac{\sigma_m}{\sigma_0}\right) + \frac{f}{2}\sinh\left(\frac{3\sigma_m}{2\sigma_0}\right)\right)\delta_{ij}\right] \quad \text{(A5)}$$

References

1. C. B. BUCKNALL, "Toughened Plastics" (Applied Science Publishers, London, 1977).
2. P. BEAHAN, A. THOMAS and M. BEVIS, *J. Mater. Sci.* **11** (1976) 1207.
3. A. M. DONALD and E. J. KRAMER, *J. Appl. Polym. Sci.* **27** (1982) 3729.
4. G. H. MICHLER, *Acta Polymerica* **36** (1985) 285.
5. R. A. BUBECK, D. J. BUCKLEY, E. J. KRAMER and H. BROWN, *J. Mater. Sci.* **26** (1991) 6249.
6. A. S. ARGON and M. M. SALAMA, *Mater. Sci. Engng* **23** (1977) 219.
7. H. BREUER, F. HAAF, and J. STABENOW, *J. Macromol. Sci.—Phys.* **B14** (1977) 387.
8. G. H. MICHLER, *Colloid Polym. Sci.* **267** (1989) 377.
9. A. F. YEE and R. A. PEARSON, *J. Mater. Sci.* **21** (1869) 2462.
10. *Idem., ibid.* **21** (1986) 2475.
11. H.-J. SUE, *ibid.* **27** (1992) 3098.
12. A. LAZZERI, PhD thesis, Cranfield Institute of Technology, Cranfield, UK (1991)
13. A. F. YEE and R. A. PEARSON, in "Fractography and Failure Mechanisms of Polymers and Composites" edited by A. C. Roulin-Moloney (Elsevier Applied Science, London, 1989) p. 291.
14. R. J. M. BORGGREVE, R. J. GAYMANS and H. M. EICHENWALD, *Polymer* **30** (1989) 78.
15. A. J. OOSTENBRINK, L. J. MOLENAAR and R. J. GAYMANS, Third European Symposium on Polymer Blends, Cambridge, 24–26 July 1990 (Plastics and Rubber Institute, London, 1990) paper E3.
16. F. RAMSTEINER, *Kunststoffe* **73**(3) (1983) 148.
17. F. RAMSTEINER and W. HECKMANN, *Polym. Commun.* **26** (1985) 199.
18. F. SPERONI, E. CASTOLDI, P. FABBRI and T. CASIRAGHI, *J. Mater. Sci.* **24** (1989) 2165.
19. C. B. BUCKNALL, P. HEATHER and A. LAZZERI, *ibid.* **24** (1989) 1489.
20. K. DIJKSTRA, PhD thesis, University of Twente, Netherlands (1993).
21. A. N. GENT and C. WANG, *J. Mater. Sci.* **26** (1991) 3392.
22. D. C. EDWARDS, *ibid.* **25** (1992) 4175.
23. H. VANGERKO and L. R. G. TRELOAR, *J. Phys. D Appl. Phys.* **11** (1978) 1969.
24. P. F. THOMASON, "Ductile Fracture of Metals" (Pergamon Press, Oxford, 1991).
25. A. L. GURSON, *J. Eng. Mater. Technol., Trans. ASME* **99** (1977) 2.
26. C. A. BERG, in "Inelastic Behaviour of Solids", edited by M. F. Kanninen (McGraw-Hill, New York, 1970) p. 171.
27. I. M. WARD, *J. Mater. Sci.* **6** (1971) 1397.
28. N. BROWN, in "Failure of Plastics", edited by W. Brostow (Hanser Publishers, Munich, 1986).
29. R. J. YOUNG and P. A. LOVELL, "Introduction to Polymers", 2nd Edn (Chapman & Hall, London, 1991).
30. A. L. GURSON, PhD thesis, Brown University (1975).
31. *Idem.*, in Proceedings of the International Conference on Fracture, ICF4 Fracture 1977, Waterloo, Canada, Vol. 2A (Pergamon Press, Oxford, 1977) p. 357.
32. R. HILL, "The Mathematical Theory of Plasticity" (The University Press, Oxford, 1950).
33. H. YAMAMOTO, *Int. J. Fract.* **14** (1978) 347.
34. P. B. BOWDEN, in "The Physics of Glassy Polymers", edited by R. N. Haward (Applied Science Publishers, London, 1973).
35. I. M. WARD, "Mechanical Properties of Solid Polymers" (Wiley, New York, 1983) p. 362.
36. J. F. W. BISHOP and R. HILL, *Phil. Mag.* **42** (1951) 414.
37. *Idem., ibid.* **42** (1951) 1298.
38. J. C. BAUWENS, *J. Polym. Sci. A-2* **5** (1967) 1145.
39. *Idem., ibid. A-2* **8** (1970) 893.
40. P. B. BOWDEN and J. A. JUKES, *J. Mater. Sci.* **7** (1972) 52.
41. A. S. ARGON, R. D. ANDREWS, J. A. GODRICK and W. WHITNEY, *J. Appl. Phys.* **39** (1968) 1899.
42. R. P. KAMBOUR, *Nature* **195** (1962) 1299.
43. *Idem., Polymer* **5** (1964) 143.
44. A. M. DONALD and E. J. KRAMER, *J. Polym. Sci. Polym. Phys.* **20** (1982) 899.
45. P. L. FERNANDO and J. G. WILLIAMS, *Polym. Engng Sci.* **20** (1980) 215.

46. O. F. YAP, Y.-W. MAI and B. COTTERELL, *J. Mater. Sci.* **18** (1983) 657.
47. E. J. KRAMER. *Polym. Engng Sci.* **24** (1984) 761.
48. S. WU, *Polymer* **26** (1985) 1855.
49. *Idem., J. Appl. Polym. Sci.* **35** (1988) 349.
50. R. J. M. BORGGREVE, R. J. GAYMANS, J. SCHUIJER and J. F. INGEN-HOUSZ, *Polymer* **28** (1987) 1489.
51. R. J. M. BORGGREVE, R. J. GAYMANS and J. SCHUIJER, *ibid.* **30** (1989) 71.

Received 5 April
and accepted 2 June 1993